Conference materials
UDC [621.793+544.164]::681.787.22
DOI: https://doi.org/10.18721/JPM.173.113

Change in the carbon nanotube thin layer refractive index after water and ammonia molecules adsorption

A.V. Romashkin [1] ✉, R.Yu. Rozanov [2], A.V. Lashkov [1], A.S. Vishnevskiy [3], A.E. Mitrofanova [2, 4], D.D. Levin [2], V.V. Svetikov [2, 5]

[1] National Research University of Electronic Technology, Zelenograd, Moscow, Russia;
[2] JSC "Zelenograd Nanotechnology Center", Zelenograd, Moscow, Russia;
[3] MIREA – Russian Technological University, Moscow, Russia;
[4] Moscow Institute of Physics and Technology, Dolgoprudny, Moscow Region, Russia;
[5] Prokhorov General Physics Institute of the RAS, Moscow, Russia
✉ romaleval@gmail.com

Abstract. Spray-deposited carboxylated carbon nanotube (CNT) layers were characterized using AFM, Raman, and spectroscopic ellipsometry. The layers' thickness, diameters and band gap of CNTs, as well as the changes in the CNT layer refractive index at 1319 nm and 2010 nm after H_2O and NH_3 adsorption in air and H_2O in N_2 were analyzed. Refractive index changes and modeling the necessary length of the modified interferometer arm for a $\pi/2$ phase shift allow us to propose the use of such CNT layers for integrated interferometric sensors and gas recognition.

Keywords: carbon nanotube, ellipsometry, integrated optics, interferometer, sensor

Funding: This research was supported by the Ministry of Science and Higher Education of the Russian Federation in the framework of state tasks FSMR-2023-0002 (spray deposition, post-processing, AFM, Raman study, CNT layers ellipsometry data analysis) and partially FSFZ-2023-0005 (RTU MIREA: CNT layer ellipsometry in N_2 with H_2O or 2-propanol vapors).

Citation: Romashkin A.V., Rozanov R.Yu., Lashkov A.V., Vishnevskiy A.S., Mitrofanova A.E., Levin D.D., Svetikov V.V., Change in the carbon nanotube thin layer refractive index after water and ammonia molecules adsorption, St. Petersburg State Polytechnical University Journal. Physics and Mathematics. 17 (3.1) (2024) 68–74. DOI: https://doi.org/10.18721/JPM.173.113

Материалы конференции
УДК [621.793+544.164]::681.787.22
DOI: https://doi.org/10.18721/JPM.173.113

Изменение показателя преломления тонкого слоя углеродных нанотрубок при адсорбции молекул воды и аммиака

А.В. Ромашкин [1] ✉, Р.Ю. Розанов [2], А.В. Лашков [1], А.С. Вишневский [3], А.Е. Митрофанова [2, 4], Д.Д. Левин [2], В.В. Светиков [2, 5]

[1] Национальный исследовательский университет «МИЭТ», г. Зеленоград, Москва, Россия;
[2] АО «Зеленоградский нанотехнологический центр», г. Зеленоград, Москва, Россия;
[3] МИРЭА – Российский технологический университет, Москва, Россия;
[4] Московский физико-технический институт (национальный исследовательский университет), г. Долгопрудный, Россия;
[5] Институт общей физики им. А. М. Прохорова РАН, Москва, Россия
✉ romaleval@gmail.com

Аннотация. Карбоксилированные углеродные нанотрубки (УНТ), нанесенные аэрозольным распылением, исследовались с помощью АСМ, комбинационного рассеяния света и спектроскопической эллипсометрии. Проанализированы толщина слоев, диаметры и запрещенная зона УНТ, изменение показателя преломления слоев в ИК диапазоне после адсорбции H_2O и NH_3 на воздухе и H_2O в N_2. Расчеты длины модифицированного плеча интерферометра для $\pi/2$ фазового сдвига позволяют предложить такие слои УНТ для изготовления интегральных интерферометрических датчиков и распознавания газов.

Ключевые слова: углеродная нанотрубка, эллипсометрия, интегральная оптика, интерферометр, сенсор

Финансирование: Работа выполнена при поддержке Минобрнауки России в рамках государственного задания FSMR-2023-0002 (нанесение, постобработка, АСМ, КР спектроскопия, анализ эллипсометрии слоев УНТ) и частично FSFZ-2023-0005 (РТУ МИРЭА: эллипсометрия слоев УНТ в сухом N_2 с парами H_2O, 2-пропанола).

Ссылка при цитировании: Ромашкин А.В., Розанов Р.Ю., Лашков А.В., Вишневский А.С., Митрофанова А.Е., Левин Д.Д., Светиков В.В. Изменение показателя преломления тонкого слоя углеродных нанотрубок при адсорбции молекул воды и аммиака // Научно-технические ведомости СПбГПУ. Физико-математические науки. 2024. Т. 17. № 3.1. С. 68–74. DOI: https://doi.org/10.18721/JPM.173.113

Introduction

Recently, instead of using a complex system with various wavelengths to detect gases based on their absorption peaks, multisensor interferometric systems for gas recognition have been demonstrated [1]. To achieve their high sensitivity, it is important to develop thin modifying layers that significantly alter their own refractive index (n) upon analyte adsorption. Sensitivity at the ppb-level (for agrunitrile), as well as recognition of volatile organic compounds using the sensor array, have already been shown [1]. High selectivity and ppm-level sensitivity for H_2S by one sensor have also been shown [2]. The development of such layers is also relevant for interferometric biosensors [3]. Modified nanocarbon materials are promising for these tasks and forming the sensor array. Carboxylation of carbon nanotubes (CNTs) provides a significant increase in the response to ammonia [4]. Also, they are capable of significantly changing their electronic structure when the adsorbed molecules change [5]. However, identifying the magnitude and mechanisms of change in the optical parameters for functionalized CNTs, such as n at different wavelengths (λ) during the various molecules adsorption, remains a relevant task and is the goal of this work. Previously, only non-functionalized CNTs were studied using ellipsometry to obtain the $n(\lambda)$ graph, without studying the effect of adsorption on $n(\lambda)$ [6, 7].

Materials and methods

We studied three samples of carboxylated CNTs (P3-SWNT, Carbon Solutions, USA [8]) with different layer thicknesses, measured by AFM (NT-MDT, Russia). The CNT diameter was evaluated [9] from the RBM-band Raman (532 nm laser, Nano Scan Technology, Russia). CNTs were spray deposited from a dispersion [10] onto a Si substrate with native oxide, followed by the residual solvent removal [11] at 90 °C. The absorption of the CNT layer was evaluated by the suppression of Raman of Si by the CNT layer at points in 1×1 mm areas. AFM and ellipsometry were performed in the same areas. Spectroscopic ellipsometry (SENTECH Instruments, Germany) was performed at angles of incidence of 75°, 70°, 65° at λ: 371–2300 nm for the layer after exposure in a chamber with H_2O at ~12500 ppm (relative humidity (RH) change from 30% to ~75%) or NH_3 at ~2000 ppm and after 25 min of desorption under normal conditions at the same sample area, but different for each analyte. Exposure to H_2O or 2-propanol (IPA) in N_2 was realized in situ during ellipsometry, only at 70°, with a 0.3 L/min flow rate, managed by gas-flow controllers. The values of n, extinction coefficient (k), and carrier concentration (p) in the

layer were estimated from the found Drude–Lorentz model parameters obtained by fitting [7] the experimental ellipsometry data. Eight oscillators were used: two pairs each to describe the E_{11} or E_{22} to describe the CNT differences in the layer; one for M_{11} and the remaining to describe the onset (over 2.5–3 eV) of the π-plasmon peak CNT [6] and an increase in absorption with photon energy [12]. The band gap of the semiconductor CNT (E_{11}), the E_{22} and M_{11} transitions were estimated from the $k(\lambda)$ graph obtained from ellipsometry data [6, 7]. E_{11} was also evaluated based on the CNT diameter estimated from Raman [9], without considering the CNT chirality indices [13]. Numerical modeling (Beam Propagation Method, RSoft CAD) was carried out to evaluate the CNT modified arm length (L_{mod}) required to achieve a $\pi/2$ phase shift in the 900×350 nm Si_3N_4 waveguide Mach–Zehnder interferometer (MZI). The electric field distribution was calculated using the EME method (ANSYS Lumerical MODE).

Results and Discussion

Spray-deposited CNTs used have functional groups and contain residual solvent before post-treatment (Fig. 1, *a*). Therefore even their resulting concentration in the layer (Fig. 1, *b*, *c*) is ca. 3 times lower than in other work [6], which determines the higher slope of the thickness on absorbance dependence (Fig. 1, *d*). The layer thicknesses were 3 nm, 17 nm, 35.5 nm (Fig. 1, *b*).

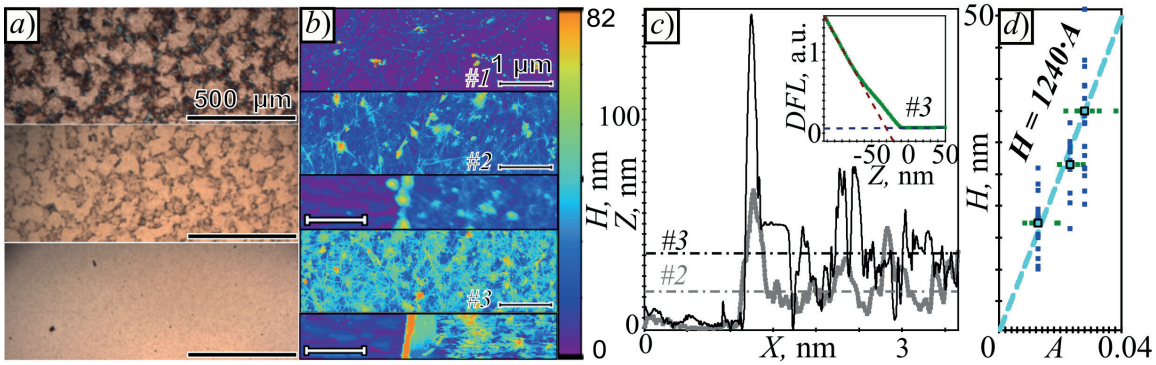

Fig. 1. Optical images of iterative residual solvent removal from the CNT layer (*a*); AFM (*b*) with cross sections, inset: force – distance curve (*c*); graph of thickness (H) versus absorbance (A) at $\lambda \approx 550$ nm (*d*)

The results of applying the Drude–Lorentz model to describe the experimental data of Ψ and Δ are shown in Fig. 2. Estimates of the n are slightly different (Fig. 2, *a*) due to the layer thickness non-uniformity (~10 %) while the thickness is the same in the model for each analyte. E_{11}, E_{22}, M_{11} evaluated from $k(\lambda)$ were 0.70, 1.31, 2.05 eV respectively, which are higher than in another work [6], due to the smaller CNT diameter. A larger M_{11} peak relative to E_{11} distinguishes functionalized CNTs [6, 12]. When exposed to H_2O in air, n increased (Fig. 2, *a*, *c*, *f*) from 1.653 to 1.661 at $\lambda = 1319$ nm (Nd:YAG laser) and from 1.890 to 1.907 at $\lambda = 2010$ nm (Tm:YAG laser). The latter λ corresponds to the photon energy, similar to E_{11} and to the estimate of the CNT band gap (E_g). Approximately 70% of the RBM Raman region (140–195 cm^{-1}) corresponds to CNT diameters of 1.6, 1.44, 1.3 nm [9] with Eg energies of about 0.67, 0.74 (~40 %), 0.81 eV [13] respectively (Fig. 2, *a* inset). The charge carrier concentration (p) decreased slightly from $5.75 \cdot 10^{19}$ cm^{-3} to $5.72 \cdot 10^{19}$ cm^{-3} when exposed to H_2O in air, which corresponds to the low resistive response of a high-density CNT network [10]. When exposed to NH_3, n dropped from 1.586 to 1.584 at $\lambda = 1319$ nm, but increased from 1.815 to 1.847 at $\lambda = 2010$ nm (Fig. 2, *a*, *d*, *g*); and p was dropped from $7.31 \cdot 10^{19}$ cm^{-3} to $7.28 \cdot 10^{19}$ cm^{-3}, which also corresponded to the low resistive response [10]. Considering the differences in the concentrations of H_2O and NH_3, the measurement results indicate a change in the electronic structure of CNTs during adsorption, and are not associated with filling the pores of the layer. This is further supported by the nature of the n response changes when the carrier gas is altered. H_2O adsorption led to an increase in the n under air conditions, but a decrease in the n when the carrier gas was dry N_2 (Fig. 2), the same as for IPA in N_2. The p values increased with the adsorption of H_2O in N_2, and for RH of 0%, 32%, 64%, 85% they were $7.55 \cdot 10^{19}$, $7.69 \cdot 10^{19}$, $7.89 \cdot 10^{19}$, $8.06 \cdot 10^{19}$ cm^{-3}. This effect is presumably

related to a charge carriers type change: from holes in air conditions to electrons in dry N_2 [6], and H_2O and NH_3 are donors for CNTs (ca. 0.03 *e*/molecule) opposed to O_2 and NO_2, both of which are charge acceptors (ca. −0.09 *e*/molecule) [14]. Thus, in air, H_2O and NH_3 reduce the concentration of CNT carriers and increase resistivity [10, 12], but in the absence of oxygen, the opposite occurs. The values of the *n*, determined after cycles of exposure to H_2O followed by N_2 purging before applying the next concentration of vapor, almost return to the initial value at 0% RH: 1.464. The values of *n* at λ = 1319 nm during exposure (subsequent purging) were: 1.453 (1.459), 1.446 (1.457), 1.431 (1.454). The incomplete return is due to incomplete desorption during 20-minute low-flow N_2 purge, which is typical for CNTs [10].

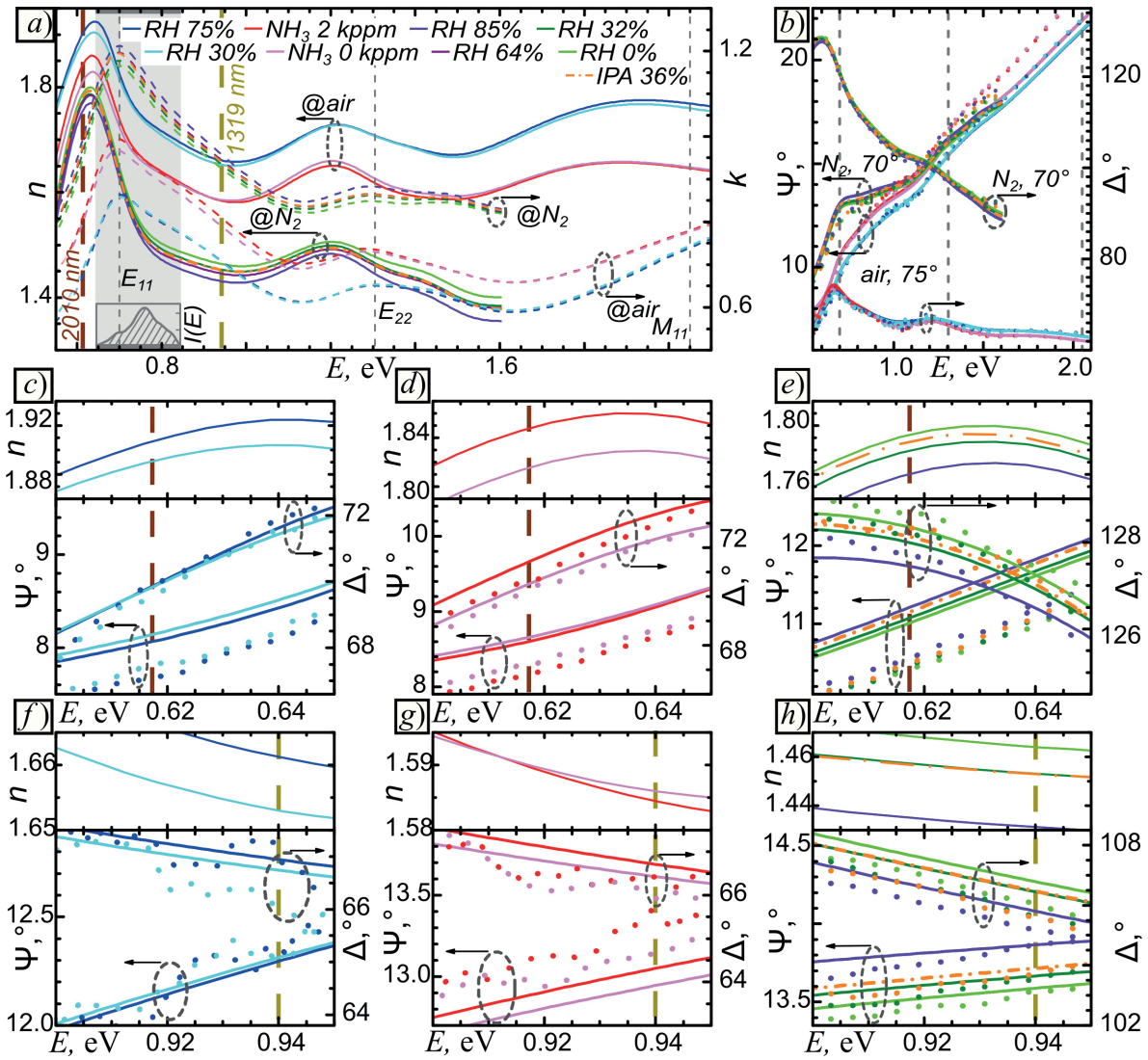

Fig. 2. Application of the Drude−Lorentz model to obtain a graph of *n* and *k* on photon energy: *n*(*E*), *k*(*E*); inset − fraction of CNT (*I*) with different E_g (*a*); to describe the experimental data of Ψ and Δ (*b*), and enlarged sections in the regions of λ = 2010 nm and λ = 1319 nm for the adsorption of H_2O (*c*, *f*) and NH_3 in air (*d*, *g*), H_2O and IPA in N_2 (*e*, *h*)

Numerical modeling showed that the single-mode regime is realized in the MZI (Fig. 3, *a*, *b*). Stronger differences in the change in *n* during NH_3 adsorption at λ = 2010 nm, compared to λ = 1319 nm (Fig. 2), determine the shorter required L_{mod} of the MZI arm: 700 μm at λ = 2010 nm instead of 7700 μm at λ = 1319 nm. Similar behavior exists for H_2O in air (Fig. 3, *c*). These obtained values are in agreement with other studies [15]. However, for H_2O vapor in N_2, more significant changes in the *n* occur in the region of 0.8−1.2 eV compared to 0.62−0.7 eV.

This enables the implementation of a π/2 phase shift using a shorter Lmod of the MZI arm: 700 μm for λ = 1319 nm instead of 780 μm at λ = 2010 nm. This is apparently due to the greater changes in the electronic structure of CNTs not near the band gap and at its edges (E_{11} region in Fig. 2 and inset), but in more distant energy regions of the CNT density of states spectrum, up to E_{22}. In turn, this can be explained by the absence of oxygen on the CNT during measurements in N_2. The absence of oxygen can alter the band structure through molecule adsorption not only the vicinity of the band gap edges but also in the region of Van Hove singularities of CNTs [16]. It apparently leads to significant changes in the $n(\lambda)$ not only in the E_{11} region but also at photon energies of 0.8–1.2 eV (Fig. 2, *a*, for NH_3 in air and H_2O in N_2), exceeding the CNT E_g energy. This corresponds to changes in the density of states no longer so much inside or near the edges of the CNT band gap but far from them, as is the case, for example, with the adsorption of NH_3 and H_2S [14, 17]. A similar behavior apparently occurs during the adsorption of H_2O in N_2. Such opposing or different changes in *n* after the adsorption of H_2O or NH_3 allow the recognition of analytes in the pair of NH_3 and H_2O in air or H_2O in air and H_2O in N_2 using the MZI configuration with two outputs by analyzing the opposing intensity changes. The intensity on each in the absence of analyte adsorption is equal to 0.5 of the sum of inputs in the signal loss absence, which sets a convenient zero point (Fig. 3, *d*, *e*).

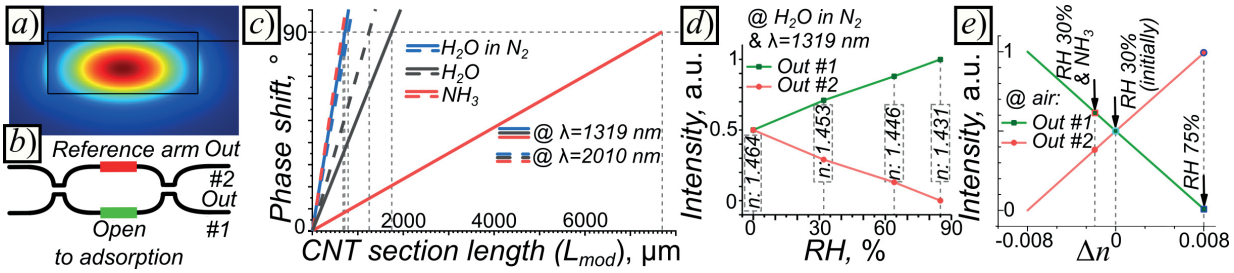

Fig. 3. Waveguide electric field distribution (*a*); MZI scheme (*b*); modified section length (L_{mod}) for π/2 phase shift (*c*); output intensities after exposure to H_2O in N_2 (d), H_2O or NH_3 in air (*e*) for selected L_{mod}

The changes in the *n* were grown when the photon energy became close to E_g (Fig. 2, *c*, *f*), thus the required L_{mod} was decreased (Fig. 3, *c*). However, due to the *n* of the CNTs becomes close to Si_3N_4, the losses in the waveguide with CNT increase (4% at λ = 1319 nm, 12% at λ = 2010 nm). The differences in the response behavior of the interferometric sensor to implement the recognition of NH_3 against the H_2O background should be noticeable already in the λ range of 1.3–1.65 μm. Based on the typical noise level in such structures of about 0.2° [1] and an estimate of the sensitivity derived from modeling and ellipsometry data of 0.045°/ppm, assuming a linear dependence of the response on concentration, we can theoretically estimate the detection limit of the proposed MZI sensor to be 4.5 ppm. This is higher than for the CNT resistive sensors [10]. However, as the CNT network density decreases, the changes in the CNT layer properties during adsorption can increase. If in resistive sensors this leads to an increase in noise that limits detection [10], in the proposed MZI sensor, high resistivity is not a limitation.

Conclusions

Spray-deposited CNT layers with subsequent solvent residual removal can be used to modify the surface of waveguides in integrated interferometric sensors. CNT layers provide high sensitivity and selectivity with maintaining an acceptable length of the interferometer arms and refractive index changes following analyte adsorption. Recognition can be realized for the NH_3 and H_2O pair in air or for the H_2O in air and H_2O in N_2 pair in the MZI configuration with two outputs, due to the opposite changes in the *n* after the adsorption of molecules in these pairs. The ability of the CNT refractive index to be changed at photon energy not near CNT band gap energy, but corresponding to the change in density of states in the CNT band structure far from the edges of the band gap with analyte adsorption opens up new additional mechanisms for increasing the sensor response and its selectivity. This can be used for the development of optical, rather than resistive,

gas sensors based on functionalized carbon nanomaterials. The low electrical conductivity of the waveguide modifying layer is not a limiting factor for the proposed MZI optical sensor. This expands the range of materials that can be used in such integrated optical sensors and potentially improves the detection limit.

REFERENCES

1. **Laplatine L., Fournier M., Gaignebet N., Hou Y., Mathey R., Herrier C., Liu J., Descloux D., Gautheron B., Livache T.,** Silicon photonic olfactory sensor based on an array of 64 biofunctionalized Mach-Zehnder interferometers, Opt. Express. 30 (19) (2022) 33955–33968.

2. **Huang G., Li Y., Chen C., Yue Z., Zhai W., Li M., Yang B.,** Hydrogen sulfide gas sensor based on titanium dioxide/amino-functionalized graphene quantum dots coated photonic crystal fiber, Journal of Physics D: Applied Physics. 53 (32) (2020) 325102.

3. **Nekrasov N., Yakunina N., Pushkarev A.V., Orlov A.V., Gadjanski I., Pesquera A., Centeno A., Zurutuza A., Nikitin P. I., Bobrinetskiy I.,** Spectral-phase interferometry detection of ochratoxin a via aptamer-functionalized graphene coated glass. Nanomaterials. 11 (1) (2021) 226.

4. **Hannon A., Lu Y., Hong H., Li J., Meyyappan M.,** Functionalized-carbon nanotube sensor for room temperature ammonia detection. Sensor Lett. 12 (10) (2014) 1469–1476.

5. **Avouris P., Martel R., Derycke V., Appenzeller J.,** Carbon nanotube transistors and logic circuits, Physica B: Condensed Matter. 323 (1–4) (2002) 6–14.

6. **Ermolaev G.A., Tsapenko A.P., Volkov V.S., Anisimov A.S., Gladush Y.G., Nasibulin A.G.,** Express determination of thickness and dielectric function of single-walled carbon nanotube films, Appl. Phys. Lett. 116 (23) (2020) 231103.

7. **Barnes T.M., Van de Lagemaat J., Levi D., Rumbles G., Coutts T.J., Weeks C.L., Britz D.A., Levitsky I., Peltola J., Glatkowski P.,** Optical characterization of highly conductive single-wall carbon-nanotube transparent electrodes, Phys. Rev. B. 75 (23) (2007) 235410.

8. **Itkis M.E., Perea D.E., Niyogi S., Rickard S.M., Hamon M.A., Hu H., Zhao B., Haddon R.C.,** Purity evaluation of as-prepared single-walled carbon nanotube soot by use of solution-phase near-IR spectroscopy, Nano Lett. 3 (3) (2003) 309–314.

9. **Zhang D., Yang J., Yang F., Li R., Li M., Ji D., Li Y.,** (n, m) Assignments and quantification for single-walled carbon nanotubes on SiO_2/Si substrates by resonant Raman spectroscopy. Nanoscale. 7 (24) (2015) 10719–10727.

10. **Romashkin A.V., Lashkov A.V., Sysoev V.V., Struchkov N.S., Alexandrov E.V., Levin D.D.,** Energy-Efficient Chemiresistive Sensor Array Based on SWCNT Networks, WO_3 Nanochannels and SWCNT-Pt Heterojunctions for NH_3 Detection against the Background Humidity, Chemosensors. 10 (11) (2022) 476.

11. **Polikarpov Y.A., Romashkin A.V., Struchkov N.S., Levin D.D.,** High uniform carbon nanotube thin films spray deposition on substrates with patterned structures having height difference, In: Proceedings of the IEEE Conference of Russian Young Researchers in Electrical and Electronic Engineering, St. Petersburg, Russia, 28–31 January 2019; IEEE. (2019) 1980.

12. **Anoshkin I.V., Nasibulin A.G., Mudimela P.R., He M., Ermolov V., Kauppinen E.I.,** Single-walled carbon nanotube networks for ethanol vapor sensing applications, Nano Research. 6 (2013) 77–86.

13. **Gelao G., Marani R., Perri A.G.,** A formula to determine energy band gap in semiconducting carbon nanotubes, ECS J. Solid State Sci. Technol. 8 (2) (2019) M19.

14. **Zhao J., Buldum A., Han J., Lu J.P.,** Gas molecule adsorption in carbon nanotubes and nanotube bundles, Nanotechnology. 13 (2) (2002) 195–200.

15. **Tseng S. Y., Fuentes-Hernandez C., Owens D., Kippelen B.,** Variable splitting ratio 2×2 MMI couplers using multimode waveguide holograms, Opt. Express. 15 (14) (2007) 9015–9021.

16. **Kroes J. M., Pietrucci F., Curioni A., Jaafar R., Gruning O., Andreoni W.,** Atomic oxygen chemisorption on carbon nanotubes revisited with theory and experiment, The Journal of Physical Chemistry C. 117 (4) (2013) 1948–1954.

17. **Tang X., Zhao Y., Liang X., Fang Z., Li X., He Y., Li H.,** Density Functional Theory Study of Adsorption and Selection Behavior of Harmful Gas Molecules on the Surface of SWNTs: Implications for Gas Sensing, ACS Appl. Nano Mater. 6 (21) (2023) 19786–19796.

THE AUTHORS

ROMASHKIN Alexey V.
romaleval@gmail.com
ORCID: 0000-0002-0101-6122

ROZANOV Roman Yu.
roman-roz@yandex.ru
ORCID: 0000-0001-5063-1669

LASHKOV Andrey V.
lav.lab-sm.sstu@rambler.ru
ORCID: 0000-0001-6794-8523

VISHNEVSKIY Alexey S.
alexeysw@mail.ru
ORCID: 0000-0002-4024-5411

MITROFANOVA Anastasia E.
mitrofanova.ae@phystech.edu
ORCID: 0009-0004-5306-278X

LEVIN Denis D.
skaldd@yandex.ru
ORCID: 0000-0002-8414-6191

SVETIKOV Vladimir V.
svetikov@nsc.gpi.ru

Received 16.07.2024. Approved after reviewing 19.07.2024. Accepted 20.07.2024.